AUTHORS' VERSION
Paper presented at:
6th International Conference on Design and Analysis of Protective Structures – DAPS 2017
November 29 - December 1, 2017, Melbourne, Australia

Numerical Sensitivity Study of Ballistic Impact on UHMWPE Composites

Christoph Grunwald[1], Torsten R. Lässig[1*], Harm van der Werff[2], Ulrich Heisserer[2],

Long Nguyen[3], Werner Riedel[1]

[1] *Fraunhofer Institute for High-Speed Dynamics, Ernst-Mach-Institut, EMI, Eckerstraße 4, D 79104, Freiburg, Germany *(torsten.laessig@emi.fraunhofer.de)*
[2] *DSM Dyneema, P.O. Box 1163, 6160 BD Geleen, NL*
[3] *Defence Science and Technology Group, 506 Lorimer St, Fishermans Bend, Victoria 3207, AUS*

Abstract

In recent years, ultra-high molecular weight polyethylene (UHMWPE) composite materials have frequently been in the spot-light of investigations for protective applications. As a result, a state-of-the-art material model with a material-characteristic discretization scheme was developed that enables a wide range of high-velocity impact simulations in hydrocodes [1, 2]. In particular, the back face deformation and the V_{50} for impact velocities above 800 m/s are reported to be well predicted when compared to ballistic impact experiments. In this study, the numerical model is applied to investigate key parameters such as sample size, strength in fiber direction and normal and shear cohesion of the bonding interfaces with regard to their influence on the back face deformation. The main part of this study is concerned with a standard 100 % crosswise layup. Chosen results for a laminate that has the back 25 % of sub-laminates helicoidally oriented with a 22.5° sequence, similar to the so-called ARL-X layup presented by [3], are compared to the results from the standard layup.

Keywords: UHMWPE, parametric study, material model, ballistic impact, interfaces

1. Introduction

In view of the rapidly increasing demand of new graded composite armor materials, UHMWPE composites set a new standard for protective applications such as vests or helmets. Their outstanding strength and stiffness to weight ratio makes them indispensable for smart protective applications in a wide field of threats, delivering increased ballistic mass efficiency with regard to the ballistic V_{50}. However, with increasing resistance, the deformation of the armor back face increases as well. This deformation is a critical factor in protective applications, since gross back face deformation (BFD) can lead to behind armor blunt trauma (BABT) or behind helmet blunt trauma (BHBT), terms which summarize serious injuries to the human body, resp. the head, evocated by high velocity impact [4]. Beyond injuries induced on the human body, the back face deformation may cause difficulties in other armor applications as well, e.g. where not enough space is available as in vehicles. The aim of composite behavior in protective applications is therefore not only the prohibition of projectile penetration, but at the same time, a reduction of the back face deformation.

In order to understand a material behavior under different conditions, numerical simulations are of great use. They can help to gain a deeper understanding of the influence of each parameter, especially in the case of composites, where different base fibers, matrix materials and architectures are used to influence certain key properties of a material. Therefore, they can play a key role in the identification of necessary property changes in order to develop optimized behavior, e.g. in regard to reduced displacement, higher energy absorption etc.

Extensive investigations on the deformation and fracture behavior of UHMWPE composites can be found in [5, 6, 7, 8, 1, 9, 10, 11]. In terms of ballistic impact situations, it was found that mechanisms such as fiber breaking, interlaminar delamination, elastic and permanent non-linear deformations are required to be considered in a numerical model to capture the energy absorption phenomena [11, 12, 13]. The mentioned phenomena were implemented by Lässig et al. [1] in a material model for monolithic bodies and further developed by Nguyen et al. [2], with focus on a sublayer discretization. These state-of-the-art approaches enabled simulations of various ballistic impact scenarios in the hydrocode Ansys

Autodyn®. The discretization of sublayers and the formulation of bonds between sub-laminates allowed realistic numerical predictions towards the ballistic V_{50} and the back face deformation of targets [2].

This study aims to numerically investigate the back face deformation, dependent on selected material parameters and target sizes of UHMWPE panels. Since recent material development tends to produce higher fiber and matrix strengths, the sensitivity of the strength in fiber direction, the interfaces' normal and shear strength, as well as the influence of the sample size on the back face deformation will be investigated for an impact of a fragment simulating projectile (FSP).

After a brief repetition of key modeling aspects, results of the parametric study for a standard [0°/90°] layout are shown and discussed (Section 3.1). An outlook on the behavior of helicoidally oriented packing is given in Section 3.2, before the study closes with a summary and conclusions.

2. Model description

In general, hydrocodes treat the pressure p and the deviatoric material response separately:

$$\boldsymbol{\sigma} = \boldsymbol{s} - p\boldsymbol{I} \quad \textbf{(1)}$$

With $\boldsymbol{\sigma}$ the full stress tensor, $p = -\frac{1}{3}tr(\boldsymbol{\sigma})$ the pressure, $\boldsymbol{s}$ the deviatoric part of the tensor and $\boldsymbol{I}$ the second order identity tensor. While the pressure is described by a so-called Equation of State (EoS) relating the pressure with other thermodynamic parameters, e.g. internal energy and density, deviatoric stresses are described by a strength model. Both parts of the material model will be explained briefly in the following sections. The model – together with a discussion of parameter choices – is described more thoroughly in [2].

2.1. *Shock Equation of state*

The above described approach of handling hydrostatic and deviatoric stresses independently assumes that deviatoric strains will not influence the volumetric response and vice versa, which is, however, not true for anisotropic material behavior. Therefore, Meyers [14] proposed a formulation based on shock physics with a limited coupling of hydrostatic and deviatoric behavior in the elastic regime:

$$p = p(\nu, e) + p(\boldsymbol{\varepsilon}_{dev}, \boldsymbol{C}). \quad (2)$$

Where $\varepsilon_{vol} = \frac{1}{3}tr(\boldsymbol{\varepsilon})$ denotes the volumetric stress, $\boldsymbol{\varepsilon}$ the strain tensor, $\boldsymbol{\varepsilon}_{dev} = \boldsymbol{\varepsilon} - \varepsilon_{vol}\boldsymbol{I}$ the deviatoric strain tensor, e the internal energy and $\boldsymbol{C}$ the rank four stiffness tensor. The shock dominated volumetric response is considered by a Mie-Grüneisen equation of state:

$$p(\nu, e) = p_r(\nu) + \frac{\Gamma(\nu)}{\nu}[e - e_r(\nu)]. \quad (3)$$

In this equation e is again the internal energy, ν the specific volume, Γ the Grüneisen-coefficient and $p_r(\nu)$ and $e_r(\nu)$ denote a reference state of pressure and inner energy respectively. Together with the well-known Rankine-Hugoniot equations (see e.g. [15, 16]) the reference state can be derived for many solid materials by a linear relationship between the shock wave velocity U_S and the particle velocity u_P:

$$U_S = c_B + Su_P, \quad (4)$$

where S is the linear slope of the U_S-u_P relationship and c_B the materials' bulk sound speed.

2.2. *Strength and failure model*

In the linear regime, stresses and strains are related to each other by the stiffness tensor **C**:

$$\boldsymbol{\sigma} = \boldsymbol{C}:\boldsymbol{\varepsilon}. \quad \textbf{(5)}$$

After the yield point has been reached, a quadratic yield function accounts for non-linear plastic deformations with hardening:

$$f(\boldsymbol{\sigma}) = a_{11}\sigma_{11}^2 + a_{22}\sigma_{22}^2 + a_{33}\sigma_{33}^2 + 2a_{12}\sigma_{11}\sigma_{22} + 2a_{23}\sigma_{22}\sigma_{33} + 2a_{13}\sigma_{11}\sigma_{33} + 2a_{44}\sigma_{23}^2 + 2a_{44}\sigma_{31}^2 + 2a_{66}\sigma_{12}^2 = k. \quad (6)$$

in which a_{ij} are constant plasticity coefficients and k the hardening parameter, see [17] for details.

Failure is initiated when a combined stress criterion reaches a threshold of one:

$$\left(\frac{\sigma_{ii}}{S_{ii}(1-D_{ii})}\right)^2 + \left(\frac{\sigma_{ij}}{S_{ij}(1-D_{ij})}\right)^2 + \left(\frac{\sigma_{ki}}{S_{ki}(1-D_{ki})}\right)^2 \geq 1 \text{ for } i,j,k = 1,2,3. \quad (7)$$

In the equation above, S_{ii} denotes the failure strength in the principal directions, S_{ij} and S_{ki} the shear failure strengths in-plane and through-thickness, respectively. Damage is considered by the damage parameter D_{ii}, which relates to the fracture-energy linearly:

$$D_{ii} = \frac{L\sigma_{ii,f}\varepsilon_{cr}}{2G_{ii,f}}. \quad (8)$$

with L the characteristic numerical element length, ε_{cr} crack strain and $G_{ii,f}$ the fracture energy in the considered direction.

2.3. *Erosion model*

Dealing with highly deformed elements in a hypervelocity context makes the application of an appropriate erosion criterion indispensable. Since the overall time step of an explicit integration scheme depends on the smallest element edge length – highly distorted elements may lead to a drastic decrease of the time step and therefore to a disproportionate increase of simulation time. Since those elements hardly contribute to the remaining overall response of the target, it is desirable to delete them from the calculation. For isotropic materials a strain-based criterion is normally used, i.e. elements are deleted when an appropriate strain value (normally the effective strain) exceeds a defined criterion. This is, however, not applicable for anisotropic materials. If failure occurs in one direction, the elements' stiffness decreases in this direction, hence large strains can develop although the element may have almost full resistance in the other principal directions. Since for composites the in-plane (fiber) strength is in general much higher than the through-thickness strength, a failure of the latter would result in high strains and accordingly, the element would be deleted, although it has not even reached the failure strain in the in-plane direction. Hence, a gross underprediction of the material stiffness would be the result. To avoid this issue, an anisotropic, damage-based erosion criterion was used in the model. Elements were only deleted if they have fully failed in the in-plane direction, which is the case when $D_{22} = D_{33} = 1$. A suitable approach for element erosion, implemented via subroutine is presented by Nguyen et al. [2].

2.4. *Cohesive zone model*

UHMWPE composites generally consist of very thin layers with [0°/90°] orientation. Four layers form a sheet and several sheets together constitute the laminate. Since the layers, and therefore the sheets, are very thin, a numerical element encompasses multiple layers in a bundle. In order to decouple the through-thickness shear from the through-thickness tensile behavior, the composite plate is divided into sub-laminates. They are each one element thick and connected no longer by shared nodes, but by a contact algorithm, which considers interface failure in in-plane shear as well as tensile failure in normal direction.

Since the contact algorithm in Ansys® Autodyn demands a small, element edge length dependent gap, the discretized sub-laminates also show gaps with a constant distance between them. The sub-laminates are kinematically joined, but are released if a combined stress criterion reaches a limit threshold of one:

$$\left(\frac{\sigma_N}{S_N}\right) + \left(\frac{\sigma_S}{S_S}\right) \geq 1. \tag{9}$$

Where σ denotes the current stress and S the failure stress. Subscripts N and S refer to normal direction and shear plane, respectively. For the sub-laminates, the through-thickness tensile limit stress S_{11} is set to a very high value to avoid failure in through-thickness direction within the elements.

3. Investigation of key strength phenomena – a parameter study

Lightweight armor systems made of UHMWPE composite materials are used for ballistic protection against a wide field of projectiles. Although the main failure mechanism for thin composite plates under impact loading is tensile failure, Nguyen [18] investigated the behavior of thick UHMWPE composites under impact by FSPs and found that the impact behavior can be described by two distinct phases. In the first phase, the projectile penetrates the layers (tensile failure of fibers), but with increasing depth of penetration, growing interlaminar failure is observed until the projectile no longer penetrates the layers. Instead, the remaining laminate deforms in a Membrane-like manner causing back face deformation (BFD). Figure 1 shows a schematic sequence of the different involved failure mechanisms of a UHMWPE composite, culminating in BFD.

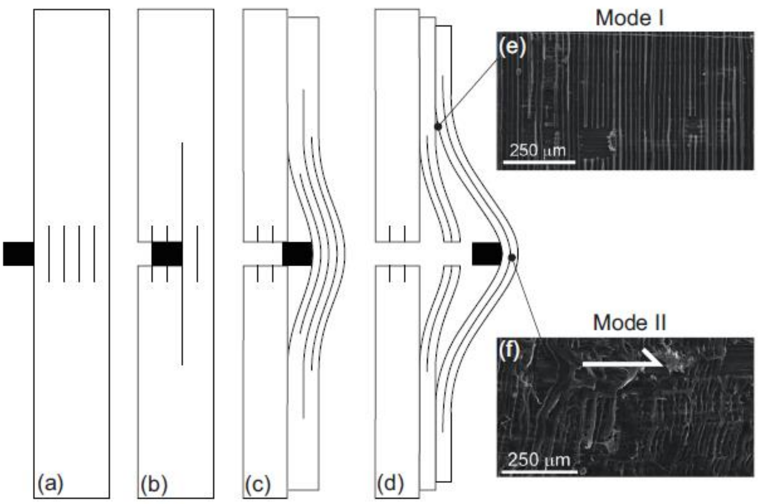

Figure 1: Failure mechanisms for impact of a FSP on a UHMWPE plate. The impact creates shock waves, which lead to bond failure around the impact axes (a). Following this phase, the projectile penetrates and the material fails under shear (b). When the release wave – the reflection of the shock wave on the free rear face – reaches the projectile, a transition between shear failure and bending is observed (c). Material is drawn in from the edges and the projectile is finally stopped by a bulge of the last material layers (d). Figure from [19].

In this study, different parameters of the Dyneema® HB26 composite were changed in the numerical model and the influence on the BFD was investigated. Nguyen [19] reported an experimental setup with a 20 mm thick and 30 × 30 cm² sized panel of the same material, clamped on a steel frame and subjected to a 20 mm FSP impact with v_i = 888 m/s. This setup was chosen as a reference configuration and modelled with the sub-laminated approach, suggested by [2], [19] in Ansys® Autodyn. Material parameters were chosen exactly as in [2], see Appendix.

For the parameter study, the following parameters were changed:

- Failure strength in fiber direction $S_{22,33}$
- the interface normal failure strength S_N
- the interface shear failure strength S_S
- the samples dimension

The initial material parameters found in [2] were multiplied by the factors of 0.5, 1 and 1.5, respectively. Furthermore, two different laminate structures were investigated for the full parameter range: one standard, crosswise layup (18 plies with [0°/90°]$_n$) and a so-called helicoidally oriented layup. In this layup, the first ¾ of the sample laminate is oriented in [0°/90°] and the remaining ¼ (4 sub-layers) is rotated by a 22.5° sequence each (Figure 2). This stacking was introduced by [20] and was found to significantly reduce the back face deformation. In this paper, however, we will discuss mainly the [0°/90°] case.

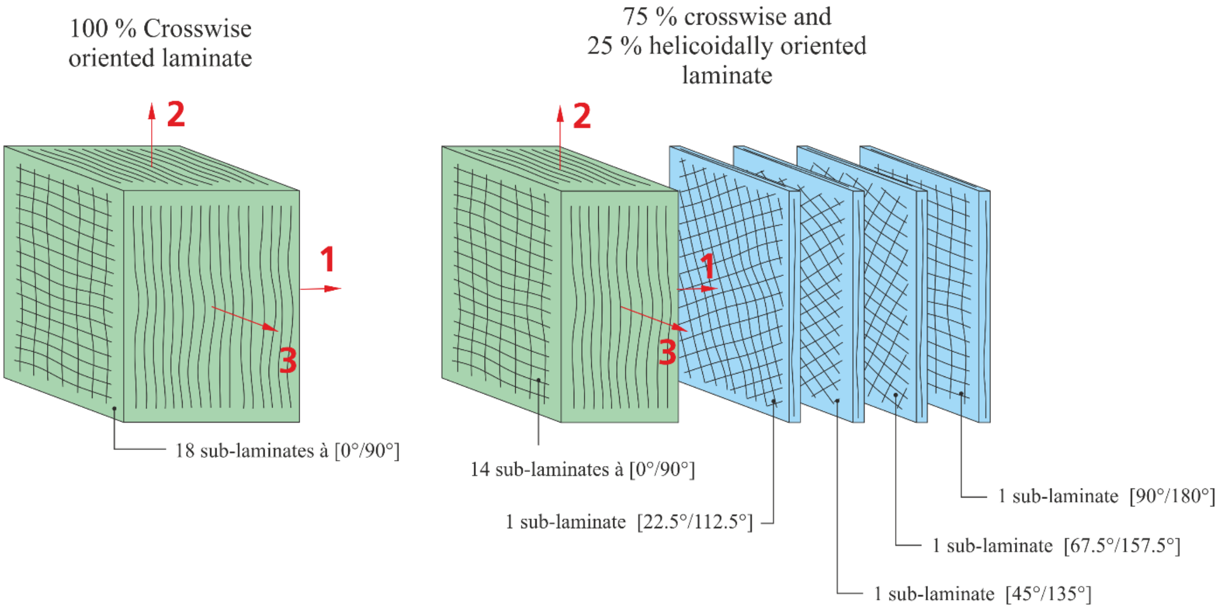

Figure 2: Crosswise (left side) and partial helicoidally oriented layup (right side) of the Dyneema© HB26 laminate, used in the parametric study.

No boundary conditions were applied on the composite. In personal armor applications, an adequate UHMWPE plate would be placed into pockets of a fabric e.g. of a vest, which means that the composite plate is neither fully constrained, nor totally free. The assumption to neglect boundary conditions is considered to be on the conservative side. Nguyen [19] also reported clamp slippage in the experiments, justifying the choice of neglecting boundaries even more.

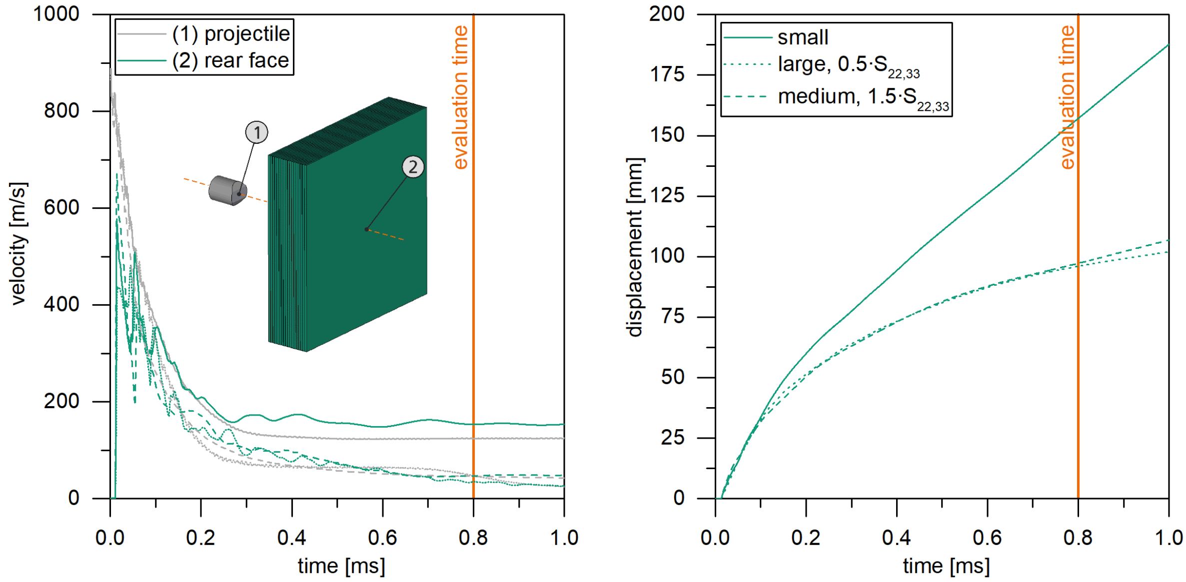

Figure 3: Evaluation of the back face deformation. Left side: Velocity history of the projectile and the center point of the rear face for three plate sizes. Right side: Integration of the velocities yields the appropriate displacement histories.

Focus of this study is to determine which parameter would lead to an effective reduction of the back face deformation. In order to compare the results, an appropriate point of time was chosen at which the velocities of the projectile and the velocity of a measurement gauge at the rear of the composite were determined for each simulation run (see Figure 3). The deformation was then determined by the integration of the velocity history at the rear's center point. Since the projectile was almost completely decelerated within the first 0.8 ms for almost all cases, the evaluation was done at t_E = 0.8 ms. However, due to the fact that the deceleration was still ongoing in some cases, the deformation evaluated at 0.8 ms cannot be seen as an absolute value, but as a relative value for the purpose of comparison. Additionally, the evaluated displacement is – strictly speaking – not pure back face deformation, but includes the rigid body displacement of the sample target plate, which is, however, negligible in almost all cases.

3.1. Crosswise oriented sub-laminates

The basic model, used in the parameter study, was 30 × 30 cm² (labeled "medium sample" in the following). In one model setup, the edge size was bisected ("small sample") and in an additional one, doubled ("large sample"). Figure 4 shows the deformation of the models after 0.8 ms:

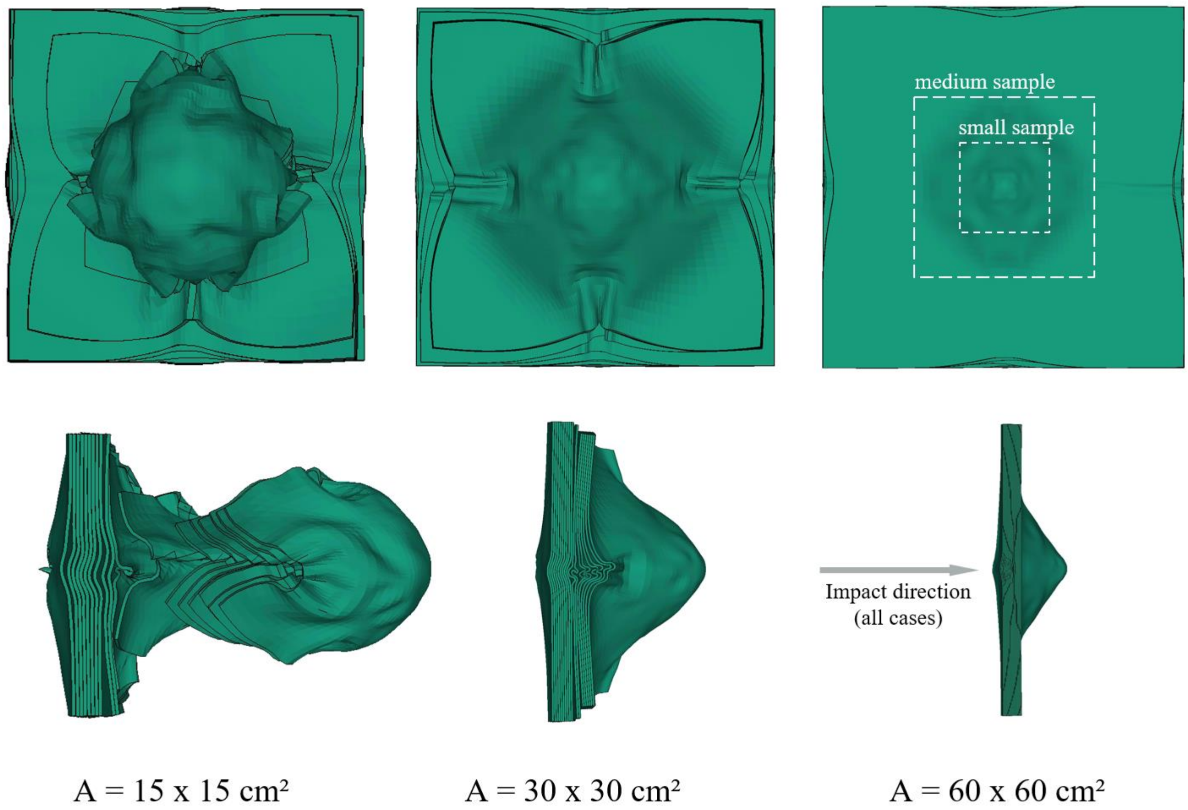

Figure 4: Impact of a 20 mm FSP with v_i = 888 m/s in a standard pack of Dyneema© HB26 with a failure strength in fiber direction of $S_{22,33}$ = 1150 MPa for different sample sizes: small (15 × 15 cm², left), medium (30 × 30 cm², center) and large (60 × 60 cm², right). View on rear face (top) and side view (bottom).

A significant influence of the sample size on the back face deformation is shown in Figure 4. One major contributing factor is the material draw-in from the edges. During bulging, the transition layer is drawn in radially from the edges – the smaller the distance between edge and penetration channel, the more material is drawn into the center. At the four nearest points to the center, the edges of the sub-laminates fold.

In case of the large sample size, almost no material is drawn in at the transition layer, hence the back face deformation is strongly reduced. In this case, the bulge is mainly the effect of elastic and plastic fiber deformations.

Besides the draw-in of material, several further aspects contribute to the back face deformation. The lack of bending stiffness leads to a membrane behavior of the sub-laminates when loaded perpendicularly. The amount of deformation is thereby mainly restricted by the interlaminar shear strength. If it is too low, plies are able to slip and each sub-laminate behaves as a single membrane. Since the interlaminar bonding is often already damaged due to the primary shock wave after projectile impact, the laminate is reduced to multiple membranes (mode I) even before bulging starts (refer to Figure 1a and 1b). Furthermore, the shear strength determines the beginning of the deflection, since the lateral constraint of the interlaminar bond directly influences the ability of the membrane to move out of plane. Finally, the strength in fiber direction influences the bulge height indirectly, since the modulus of the yarn increases with strength.

3.1.1. Variation of strength in fiber direction

The strength in fiber direction was set to be $0.5{\cdot}S_{22,33}$, $1.0{\cdot}S_{22,33,}$ and $1.5{\cdot}S_{22,33}$ with $S_{22,33} = 1150$ MPa [2]. Although the shear strength $S_{12,31}$ was chosen to be $S_{22,33}/2$ in the original formulation, this parameter was kept constant to reduce the number of influences on the results.

Figure 5 shows the deformation at 0.8 ms for the “normal” plate size (30 × 30 cm²). In case of the reduced strength in fiber direction, a perforation occurred (projectile not shown). The same was observed for all other cases with $0.5{\cdot}S_{22,33}$, regardless of the sample plates’ size or the other varying parameters. At the same time, it was already observable that an increase of the strength in the fiber direction, e.g. by stronger fibers, lead to a decreased back face deformation.

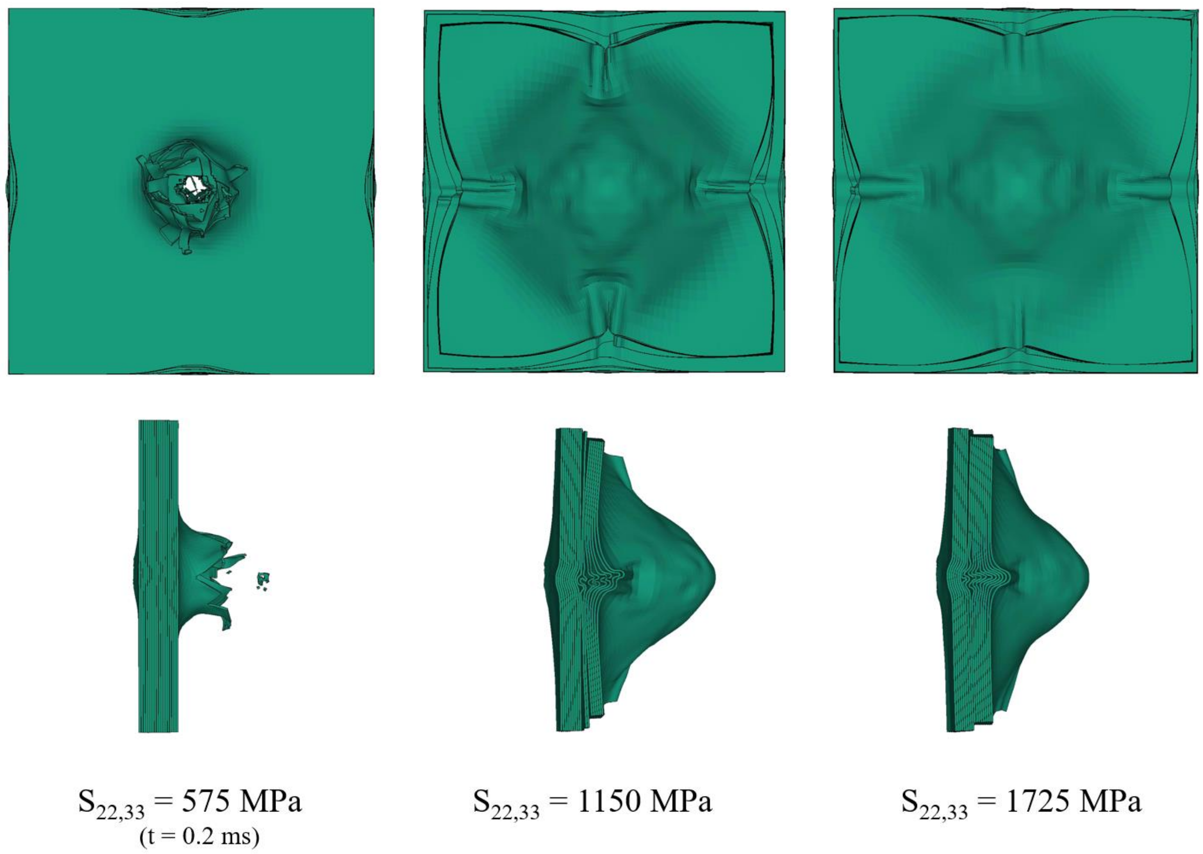

Figure 5: Impact of a 20 mm FSP with v_i = 888 m/s onto the Dyneema© HB26 laminate of medium size (30 × 30 cm,) varying strength in fiber direction. Rear view (top) and side view (bottom).

A more quantitative comparison of the back face deformation is given in the diagrams of Figure 6. The absolute values of the BFD are shown in the left diagram, whereas the right side shows the ratio of the change of the BFD compared to the reference case (medium sample size with parameter given by [2]).

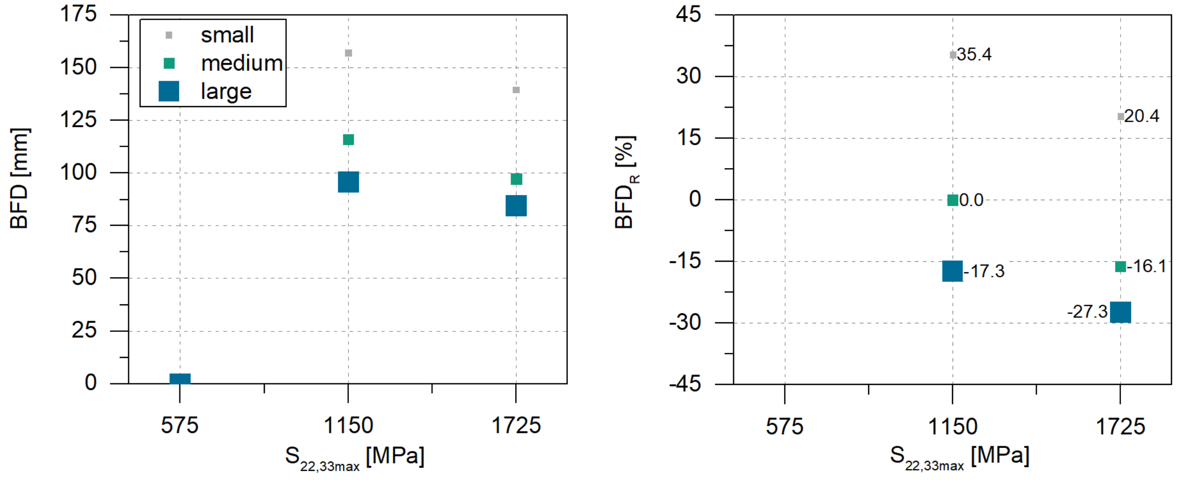

Figure 6: Variation of the back face deformation (BFD) for three different sample sizes and strength in the fiber direction. Left side: absolute values where 0 mm BFD indicates perforation, Right side: relative values. 0 % is the BFD of the reference configuration.

From this diagram, it is observable that a 150 % increase of the strength in fiber direction lead in the simulations to a reduction of the BFD of -16.1 % for the normal-sized plate (green squares, compare horizontally), -15.0 % of the small-sized plate (grey squares) and a -10.0 % reduction in case of the large sheet (blue squares). Considering the influence of the sheet size only, the increase of BFD for the small size compared to the standard size was +35.4 % for $S_{22,33}$ = 1150 MPa and +36.5 % for $S_{22,33}$ = 1725 (compare green and gray squares vertically). The BFD was reduced by -17.3 if the edge size was doubled for $S_{22,33}$ = 1150 MPa, but only reduced by -11.2 % if considering the higher strength of $S_{22,33}$ = 1725 MPa (compare green and blue squares vertically).

At least two things can be deduced from this comparison. First, for the two smaller samples, the simulated BFD is influenced more or less proportionately by the increase of the strength in fiber direction (around 15 %) and for the sample size at both strengths (> 35 %). However, the influence of the sample size is almost twice as high as the influence of the increased strength. Second, both influences decrease, when considering the larger sample size. The decrease of the BFD from normal to large sample size is still larger (-17.3 %) than the decrease in case of the increased strength for the large sample (-11.7 %). This leads to the conclusion that the sample size is the main contributing factor of the BFD and most effective for the smaller samples.

3.1.2. Variation of interface strength in normal direction

The interface strength in normal direction was varied accordingly to be $0.5 \cdot S_N$, $1.0 \cdot S_N$ and $1.5 \cdot S_N$ with S_N = 5.35 MPa [2]. In the diagram in Figure 7, all simulation results are plotted, except the ones with the low strength in fiber direction ($0.5 \cdot S_{22,33}$) where a full perforation was simulated for all of these cases. Square symbols stand for the standard strength in fiber direction $S_{22,33}$, whereas cross symbols denote simulation runs with an increased strength of $1.5 \cdot S_{22,33}$. The sizes and colors of the symbols relate to the sample size (gray “half-size”, green “normal-size” and blue “double-size”).

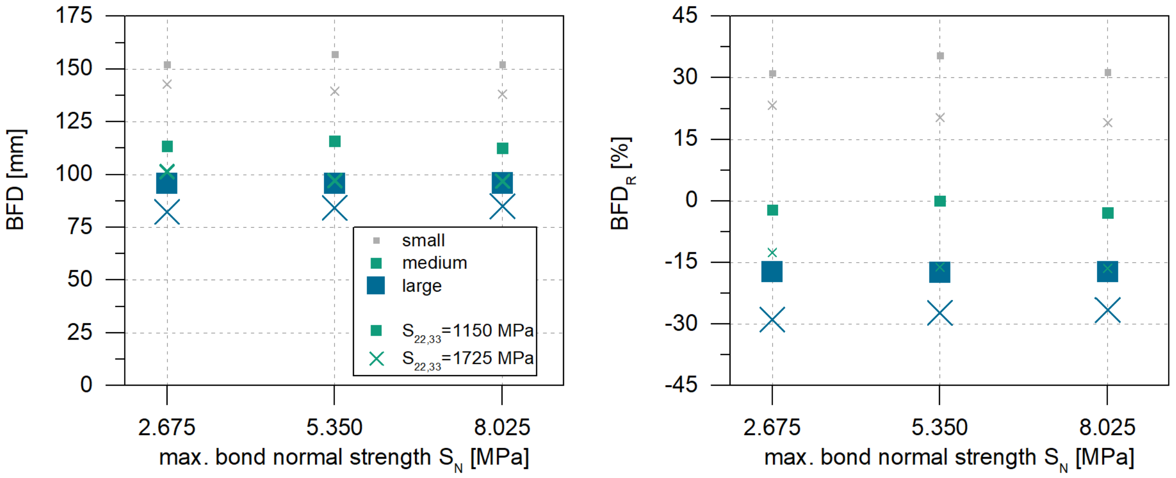

Figure 7: Variation of the bulge height (back face deformation) for three different sample sizes and variation of the strength in fiber direction, as well as the interface strength in normal direction. Left: absolute values, Right: relative values. 0 % is the bulge height of the reference configuration.

From Figure 7 it is obvious that the effect of an increased interface strength normal to the fiber direction is less pronounced and irregular for the different cases. The largest deviations in BFD are determined for the "small size" samples (gray squares) and are around ±4.3 %. The smallest deviation, with only 0.1 %, occur with the large samples. It is noticeable that regardless of whether the interface strength in the normal direction is increased or decreased, a reduction of BFD is typically observed. The reason for this is a numerically induced asymmetry in the simulated structural behavior. From Figure 4, it is possible to deduce that the response of the structure is not purely symmetric with regard to the corner position of the individual layers. In some of the above mentioned simulations, the projectile becomes instable and rotates in the last period of the process. This is especially pronounced in cases of the smaller samples, where large portions of the material are drawn in. Although this means that the BFD is not fully comparable between those cases, it highlights the scatter of this whole sensitivity study, which can be estimated to be around ± 4 % for the small sample, about ± 3.5 % for the standard size, and ± 2 % for the large sample.

3.1.3. Variation of interface shear strength

Finally, the interface shear strength was changed in four steps to be $0.5 \cdot S_S$, $1.0 \cdot S_S$, $1.5 \cdot S_S$ and $4.0 \cdot S_S$ with $S_S = 7.83$ MPa [2]. Since the interface shear strength is assumed to play a decisive role considering material draw in, the $4.0 \cdot S_S$ case was introduced to investigate the effect of a drastic increase. Figure 8 shows the top view on the normal sample size after 0.8 ms for the first three values of the varied parameter. From this figure, it is observable that the material draw-in from the outer sides is already reduced.

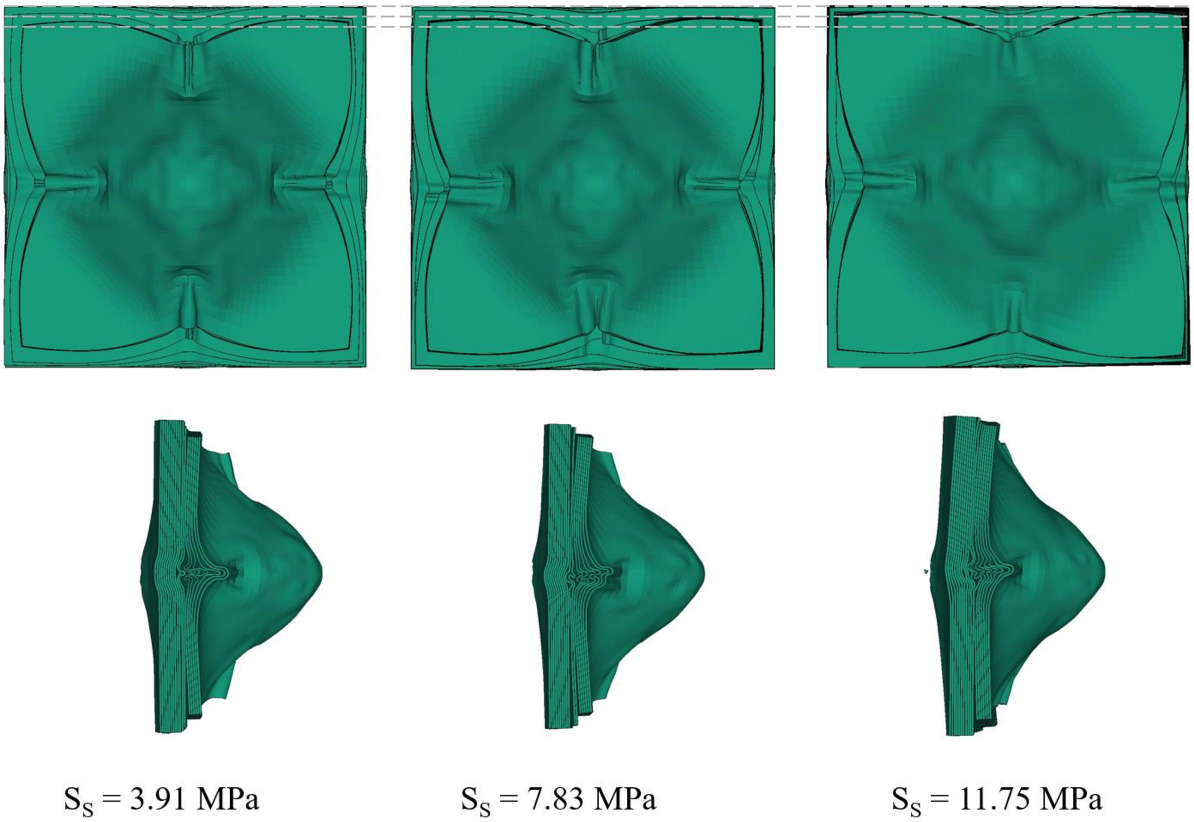

Figure 8: Impact of a 20 mm FSP with v_i = 888 m/s onto the Dyneema© HB26 laminate of medium size (30 × 30 cm,) with standard strength in fiber direction ($S_{22,33}$ = 1125 MPa) and varying the interface shear strength S_S. Rear view (top) and side view (bottom).

The diagrams with the actual values of the BFD are shown in Figure 9. The decrease of the BFD, dependent on the increased interface shear strength, is clearly visible, although some outliers can be seen. In these cases, the asymmetric failure behavior explained in the section above (see, e.g. the right top view in Figure 8 where an asymmetric deformation is observable) may have led to a rotation of the projectile within the sample and, thereby, influenced the final deformation.

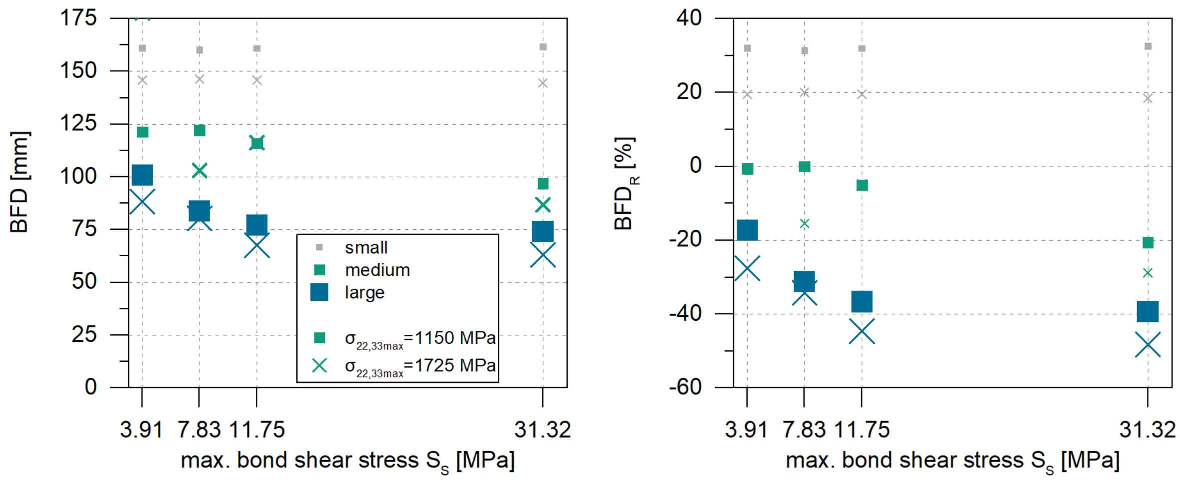

Figure 9: Variation of the back face deformation for three different sample sizes and variation of the strength in fiber direction, as well as the interface shear strength. Left: absolute values, Right: relative values. 0 % is the BFD of the reference configuration.

The values in Figure 9 indicate that the decrease of BFD follows the increase of interlaminar shear strength non-linearly. A more pronounced drop from $1.0 \cdot S_S$ (7.83 MPa) to $1.5 \cdot S_S$ (11.75 MPa) can be seen in comparison to the change of BFD from $0.5 \cdot S_S$ (3.91 MPa) to $1.0 \cdot S_S$ (7.83 MPa). It is furthermore observable that the increased strength has almost no effect for the small sample size.

3.2. 75 % crosswise and 25 % helicoidally oriented sub-laminates

Vargas-Gonzales et al. investigated the ballistic V_{50} and the BFD for different fiber orientations and architectures [3], [21]. Trying to reduce the BFD while maintaining the V_{50} of a standard layup, they created an architecture, where the first 75 % of the target consisted of crosswise [0°/90°] and the remaining 25 % of helicoidally oriented sub-laminates, in which each two [0°/90°] plies were rotated by 22.5° to its antecedent (see Figure 2). They reported a significant decrease of the BFD, up to 40% compared to standard crosswise layup. Hazzard et al. [20] worked with a fully helicoidally layup of very thin targets, where each ply was rotated by 11.5° to its antecedent, and found the effect of reduced back face deformation for hemispherical projectiles as well.

In our numerical study, the helicoidally oriented layup was achieved by rotating the material coordinate system of the last four sub-laminates by 22.5° each. Therefore, the layup was built up with 14 sub-laminates in [0°/90°] (green) and four sub-laminates with [22.5°/112.5°] (turquoise), [45°/135°] (red), [67.5°/ 157.5°] (pink) and [90°/180°] (yellow), respectively, see Figure 10.

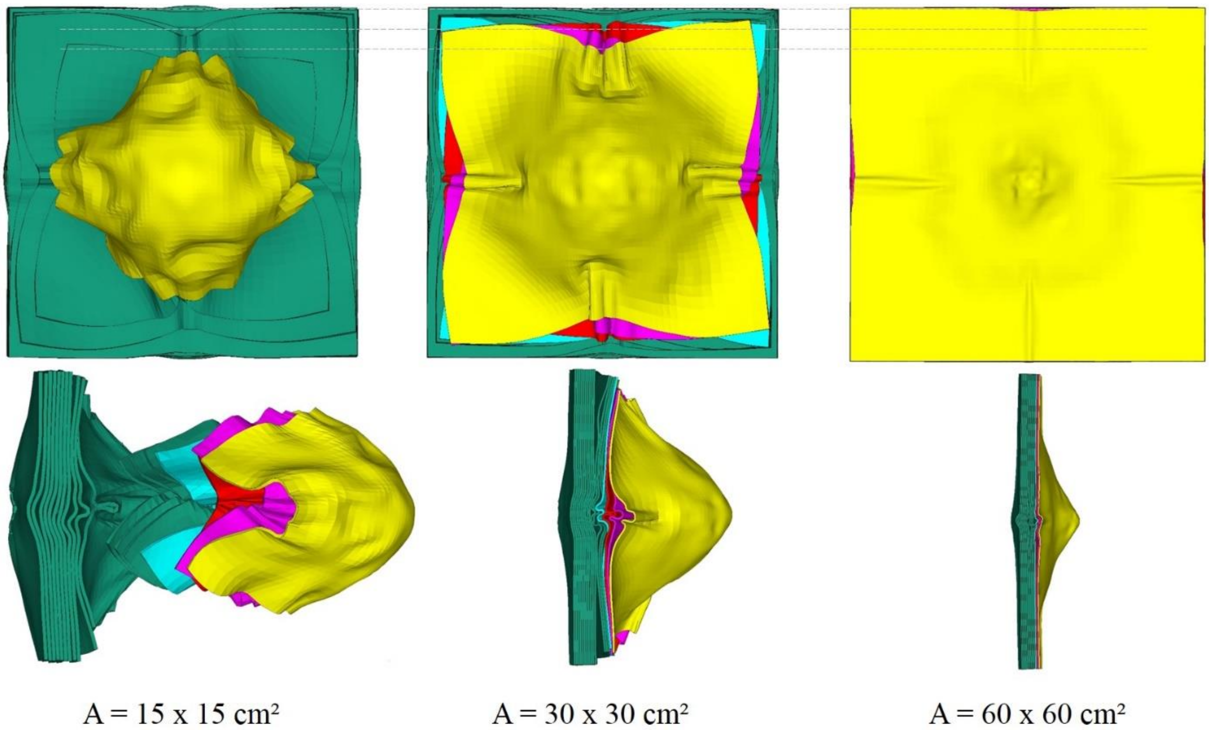

Figure 10: Impact of a 20 mm FSP with v_{imp} = 888 m/s on Dyneema® HB26 with 75 % crosswise and 25 % helicoidally oriented sub-laminates, varying the sample sizes.

A direct comparison between the BFD for the crosswise (subscript "cw") and for the partly, helicoidally oriented laminates (subscript "hc") is shown in Figure 11. The left part of the diagram shows a compilation of the absolute values of the BFD for a variation of the sample size and the strength in fiber direction. The right side of Figure 11 shows the ratio of the BFD for the crosswise to the partly, helicoidally oriented laminate, as:

$$BFD_R = \left(\frac{BFD_{CW} - BFD_{HC}}{BFD_{CW}}\right) \cdot 100$$

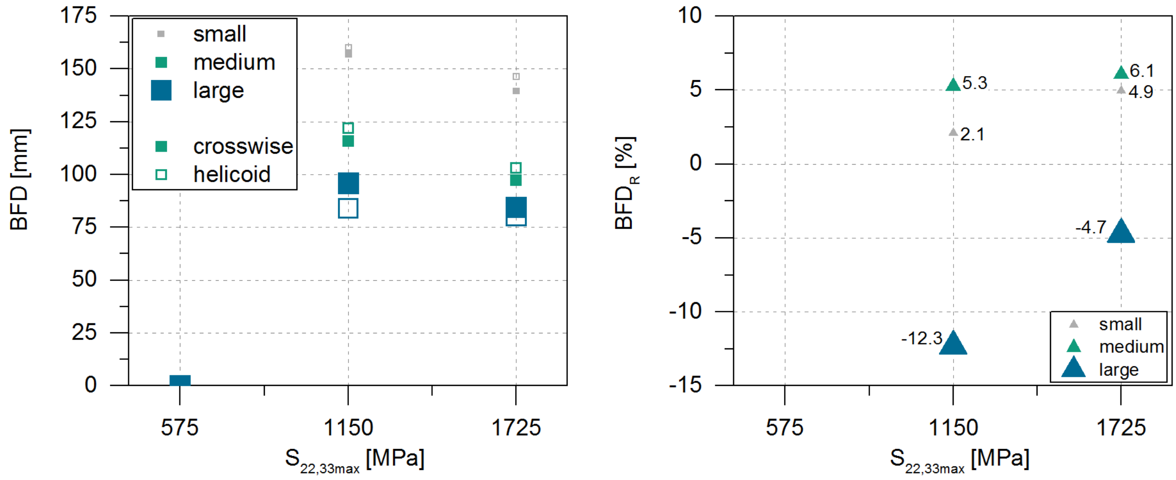

Figure 11: Comparison of the back face deformation between standard (crosswise) and helicoidally oriented sub-laminates. Left: Absolute value; Right: relative values

The numerical results show a reduction of the BFD only for the large sample, with a maximum of -12.3 %. In case of the small- and the medium-sized samples, the simulations predict an even higher BFD than as for the crosswise laminate. Obviously, the overall approach is not able to cover the positive effects of a helicoidally oriented architecture, although it is currently unknown where the limitations are. From a current perspective, it is assumed that the simple interface condition between the layers is not able to cover the complex delamination behavior, such as fiber bridging, between rotated layers sufficiently enough.

4. Summary and conclusions

In this study, the material model and the discretization methodology presented by Nguyen et al. [2] was applied to the impact of an 20 mm FSP with $v_i = 888$ m/s on a 20 mm thick UHMWPE target. Aim of the study was to investigate the influence of selected parameters with regard to the back face deformation. The structure was discretized with solid element sub-laminates, connected with a stress based interface failure criterion.

The targets dimensions, the strength in fiber direction, the interface strength in normal direction and the interface shear strength were varied and the back face deformation recorded. In addition to variations of the parameters, the standard crosswise layup [0°/90°] and a partially helicoidally oriented layup were numerically investigated in regards to the influence of fiber orientation.

With regard to the standard [0°/90°] crosswise layup, the following conclusions can be drawn concerning the influence on the back face deformation (BFD) of different model parameters:

- The size of the sample has the largest influence on reducing the BFD. For larger samples, the effect of the size decreases.
- The second most important factor is the strength in fiber direction. A higher value leads to a reduced BFD, whereas lower strength promotes a complete penetration of the sample.
- The reduction of the BFD for both parameters is not linearly proportional to the amount of parameter change. In case of the in fiber direction strength an increase about 50 % leads only to a decrease in BFD of a maximum of 15 % (depending on the sample size). The doubling of the sample edge size (thereby increasing the sample area four times) yields only a reduction of BFD around 35 % in the best case.
- The interface shear strength has an influence on the BFD, but it is less pronounced than the other two before mentioned effects and does not affect the results for the smaller samples.
- Finally, almost no significant influence on the BFD is observed by change of the interface strength in the normal direction.

Considering the helicoidally layup, the reported significant reduction of the BFD compared to the standard layup was not reproduced numerically. It should be investigated further if this conclusion can be drawn also for different impact conditions and whether more complex interface criteria are necessary to capture the energy dissipation mechanisms of this new UHMWPE target type.

References

[1] T. Lässig, L. Nguyen, M. May, W. Riedel, S. Hiermaier, U. Heisserer and H. van der Werff, A non-linear orthotropic hydrocode model for ultra-high molecular weight polyethylene in impact simulations, *Int. J. Impact. Eng.,* vol. 75, pp. 110-122, 2015.

[2] L. H. Nguyen, T. R. Lässig, S. Ryan, W. Riedel, A. P. Mouritz and A. C. Orifici, A methodology for hydrocode analysis of ultra-high molecular weight polyethylene composite under ballistic impact, *Compos. Part A-Appl. S.,* vol. 84, pp. 224-235, 2016.

[3] L. Vargas-Gonzales, Analysis of ARL X Hybrid Impact Behavior with Varying Angle Offset, in *Proceedings of the CAMX Dallas*, Texas, USA, 2015.

[4] C. J. Freitas, J. T. Mathis, N. Scott, R. P. Bigger and J. MacKiewicz, Dynamic Response Due to Behind Helmet Blunt Trauma Measured with a Human Head Surrogate, *International Journal of Medical Sciences,* no. 11(5), pp. 409-425, 2014.

[5] D. J. Chapman, C. H. Braithwaite and W. G. Proud, The response of Dyneema to shock-loading, in *Aip. Conf. Proc.,* Nashville, TN, 2009.

[6] T. K. Cwik, L. Iannucci, P. Curtis and D. Pope, Investigations of the ballistic performance of Ultra High Molecular Weight Polyethylene composite panels, Elsevier, London, UK, 2013.

[7] M. K. Hazzard, P. T. Curtis, L. Iannucci, S. Hallett and R. Trask, An investigation of in-plane performance of ultra-high molecular weight polyethylene composites, in *20th International Conference on Composite Materials,* Copenhagen, Dänemark, 2015.

[8] M. R. O'Masta, V. S. Despande and H. N. G. Wadley, Mechanisms of projectile penetration in Dyneema® encapsulated aluminum structures, *Int. J. Impact Eng.,* vol. 74, pp. 16-35, 2014.

[9] M. May, T. R. Lässig and S. J. Hiermaier, An investigation on the influence of loading rate on the fracture toughness of UHMW-PE composites, in *Proceedings of the 17th European Conference on Composite Materials,* München, 2016.

[10] T. R. Lässig, F. Nolte, W. Riedel and M. May, An assessment of experimental techniques for measuring the mode I fracture toughness of UHMW-PE composites, in *Proceedings of the 17th European Conference on Composite Materials,* München, 2016.

[11] M. J. Iremonger and A. C. Went, Ballistic impact of fibre composite armours by fragment-simulating projectiles, *Compos. Part A-Appl. S.,* vol. 27 A, pp. 575-581, 1996.

[12] E. S. Greenhalgh, V. M. Bloodworth, L. Iannucci and D. Pope, Fractrographic observations on Dyneema® composites under ballistic impact, *Compos. Part A-Appl. S.,* vol. 44, pp. 51-62, 2013.

[13] K. Karthikeyan and B. P. Russel, Polyethylene ballistic laminates: Failure mechanics and interface effect, *Mater. Design,* vol. 63, pp. 115-125, 2014.

[14] M. A. Meyers, Dynamic behavior of materials, New York: John Wiley & Sons-Verlag, 1994.

[15] W. J. M. Rankine, On the thermodynamic theory of waves of finite longitudinal disturbances, *Phil. Trans. R. Soc. B,* vol. 160, pp. 277-288, 1870.

[16] H. Hugoniot, Mémoire sur la propagation des mouvments dans les corps et spécialement dans les gaz parfaits (première partie) [Memoir on the propagation of movements in bodies, especially perfect gases (first part)], *J. Ec. Poly.,* vol. 57, pp. 3-97, 1889.

[17] R. A. Clegg, D. M. White, W. Riedel and W. Harwick, Hypervelocity impact damage prediction in composites: Part I - material model and characterization, *Int. J. Impact Eng.,* vol. 33, pp. 190-200, 2006.

[18] L. H. Nguyen, S. Ryan, S. J. Cimpoeru, A. P. Mouritz and A. C. Orifici, The effect of target thickness on the ballistic performance of ultra high molecular weight polyethylene composite, *Int. J. Impact. Eng.*, vol. 75, pp. 174-183, 2015.

[19] L. Nguyen, The Ballistic Performance of Thick Ultra High Molecular Weight Polyethylene Composite, Dissertation. Royal Melbourne Institute of Technology, School of Aerospace, Mechanical and Manufacturing Engineering, Melbourne, 2015.

[20] M. K. Hazzard, S. Hallet, P. T. Curtis, L. Iannucci and R. S. Trask, Effect of fibre orientation on the low velocity impact response of thin Dyneema® composite laminates, *Int J Impact Eng*, vol. 100, pp. 35-45, 2017.

[21] L. Vargas-Gonzales, S. M. Walsh and J. C. Gurganus, Examining the Relationship Between Ballistic and Structural Properties of Lightweight Thermoplastic Unidirectional Composite Laminates, in *SAMPE Proceedings, 17.-20.October*, Fort Worth, TX, 2011.

[22] T. Lässig, W. Riedel, U. Heisserer, H. van der Werff, M. May and S. J. Hiermaier, Numerical sensitivity studies of a UHMWPE composite for ballistic protection, in *Environment, WIT Transactions on the built environment*, Ashurst, Southampton, UK, 2014.

[23] M. May, Numerical evaluation of cohesive zone models for modeling impact induced delamination in composite materials, *Compos. Struct.*, vol. 133, pp. 16-21, 2015.

Appendix

Table 1: Input parameter for HB26 material model, according to [2]. Parameters marked with an asterisk (*) are varied in the above study.

Reference density	9.80000E-01 [g/cm3]
Youngs Modulus 11	3.62000E+06 [kPa]
Youngs Modulus 22	5.11000E+07 [kPa]
Youngs Modulus 33	5.11000E+07 [kPa]
Poissons Ratio 12	1.30000E-02 [-]
Poissons Ratio 23	0.00000E+00 [-]
Poissons Ratio 31	5.00000E-01 [-]
Shear Modulus 12	2.00000E+06 [kPa]
Shear Modulus 23	1.91800E+05 [kPa]
Shear Modulus 31	2.00000E+06 [kPa]
Gruneisen coefficient	1.64000E+00 [-]
Parameter C1	3.57413E+03 [m/s]
Parameter S1	1.30000E+00 [-]
Parameter Quadratic S2	0.00000E+00 [s/m]
Relative volume, VE/V0	0.00000E+00 [-]
Relative volume, VB/V0	0.00000E+00 [-]
Parameter C2	0.00000E+00 [m/s]
Parameter S2	0.00000E+00 [-]
Reference Temperature	2.93000E+02 [K]
Specific Heat	1.85000E+03 [J/kgK]
Thermal Conductivity	0.00000E+00 [J/mKs]
Strength	*Orthotropic Yield*
A11	1.60000E-02 [-]
A22	6.00000E-04 [-]
A33	6.00000E-04 [-]
A12	0.00000E+00 [-]
A13	0.00000E+00 [-]
A23	0.00000E+00 [-]
A44	1.00000E+00 [-]
A55	1.70000E+00 [-]

A66	1.70000E+00 [-]
Eff. Stress #1	1.47650E+03 [kPa]
Eff. Stress #2	7.00000E+03 [kPa]
Eff. Stress #3	2.70000E+04 [kPa]
Eff. Stress #4	4.00000E+04 [kPa]
Eff. Stress #5	5.00000E+04 [kPa]
Eff. Stress #6	6.00000E+04 [kPa]
Eff. Stress #7	8.00000E+04 [kPa]
Eff. Stress #8	9.80000E+04 [kPa]
Eff. Stress #9	2.00000E+05 [kPa]
Eff. Stress #10	1.00000E+06 [kPa]
Eff. Plastic Strain #1	0.00000E+00 [-]
Eff. Plastic Strain #2	1.00000E-02 [-]
Eff. Plastic Strain #3	1.00000E-01 [-]
Eff. Plastic Strain #4	1.50000E-01 [-]
Eff. Plastic Strain #5	1.75000E-01 [-]
Eff. Plastic Strain #6	1.90000E-01 [-]
Eff. Plastic Strain #7	2.00000E-01 [-]
Eff. Plastic Strain #8	2.05000E-01 [-]
Eff. Plastic Strain #9	2.10000E-01 [-]
Eff. Plastic Strain #10	2.15000E-01 [-]
Tensile Failure Stress 11	1.01000E+20 [kPa]
Tensile Failure Stress 22*	1.15000E+06 [kPa]
Tensile Failure Stress 33*	1.15000E+06 [kPa]
Maximum Shear Stress 12	5.75000E+05 [kPa]
Maximum Shear Stress 23	1.20000E+05 [kPa]
Maximum Shear Stress 31	5.75000E+05 [kPa]
Fracture Energy 11	7.90000E+02 [J/m2]
Fracture Energy 22	3.00000E+01 [J/m2]
Fracture Energy 33	3.00000E+01 [J/m2]
Fracture Energy 12	1.46000E+03 [J/m2]
Fracture Energy 23	1.46000E+03 [J/m2]
Fracture Energy 31	1.46000E+03 [J/m2]
Damage Coupling Coefficient	0.00000E+00 [-]
Interface model	
Normal Stress Limit*	5.35E+03 [kPa]
Shear Stress Limit*	7.83E+03 [kPa]